Journal of Biomedical Optics

SPIEDigitalLibrary.org/jbo

Improved light collection and wavelet de-noising enable quantification of cerebral blood flow and oxygen metabolism by a low-cost, off-the-shelf spectrometer

Mamadou Diop
Eric Wright
Vladislav Toronov
Ting-Yim Lee
Keith St. Lawrence

SPIE

Improved light collection and wavelet de-noising enable quantification of cerebral blood flow and oxygen metabolism by a low-cost, off-the-shelf spectrometer

Mamadou Diop,[a,b,*] Eric Wright,[a,b] Vladislav Toronov,[c] Ting-Yim Lee,[a,b,d] and Keith St. Lawrence[a,b]
[a]Lawson Health Research Institute, Imaging Program, London, Ontario, Canada
[b]Western University, Department of Medical Biophysics, London, Ontario, Canada
[c]Ryerson University, Department of Physics, Toronto, Ontario, Canada
[d]Robarts Research Institute, Imaging Research Laboratories, London, Ontario, Canada

Abstract. Broadband continuous-wave near-infrared spectroscopy (CW-NIRS) is an attractive alternative to time-resolved and frequency-domain techniques for quantifying cerebral blood flow (CBF) and oxygen metabolism in newborns. However, efficient light collection is critical to broadband CW-NIRS since only a small fraction of the injected light emerges from any given area of the scalp. Light collection is typically improved by optimizing the contact area between the detection system and the skin by means of light guides with large detection surface. Since the form-factor of these light guides do not match the entrance of commercial spectrometers, which are usually equipped with a narrow slit to improve their spectral resolution, broadband NIRS spectrometers are typically custom-built. Nonetheless, off-the-shelf spectrometers have attractive advantages compared to custom-made units, such as low cost, small footprint, and wide availability. We demonstrate that off-the-shelf spectrometers can be easily converted into suitable instruments for deep tissue spectroscopy by improving light collection, while maintaining good spectral resolution, and reducing measurement noise. The ability of this approach to provide reliable cerebral hemodynamics was illustrated in a piglet by measuring CBF and oxygen metabolism under different anesthetic regimens.
[DOI: 10.1117/1.JBO.19.5.057007]

Keywords: broadband near-infrared spectroscopy; cerebral oxygenation; spectrometer; CCD noise; wavelet de-noising.

Paper 140065PR received Feb. 20, 2014; revised manuscript received Mar. 27, 2014; accepted for publication Apr. 8, 2014; published online May 12, 2014.

1 Introduction

Prevention of brain injury during the perinatal period remains a primary concern in neonatal intensive care practice due to potentially devastating and life-long neurological consequences.[1] Near-infrared spectroscopy (NIRS) has been considered an ideal tool for bedside brain monitoring in newborns due to its portability, safety, and sensitivity to deep tissue oxygenation and hemodynamics.[2] As well, the relatively thin layer of superficial tissues on the newborn's head circumvents problems associated with extra-cerebral signal contamination, which is a major obstacle to adult studies.[3–5] However, quantification of cerebral oxygenation and hemodynamics by NIRS requires separating the effects of light scatter from absorption.

Time and frequency domain NIRS methods have been developed to separate scattering and absorption effects, but the instrumentations are relatively expensive and complex.[6,7] A cheaper and technically simpler approach is continuous-wave (CW) broadband NIRS.[8] Acquisition of broadband spectra has the added advantage of allowing simultaneous quantification of multiple chromophores.[9,10] With this technique, the concentrations of tissue chromophores, both endogenous and exogenous, are quantified by first or second differential analyses, which exploit the hyper-spectral content of the measurements. This approach has been shown to provide accurate measurements of cerebral blood flow (CBF) and oxygen metabolism in a neonatal animal model (piglets).[11–13] More recently, it has been adapted to clinical studies to investigate potential pharmacological effects on cerebral hemodynamics and metabolism in preterm infants.[14]

Critical to broadband CW-NIRS monitoring is efficient light collection since only a small fraction of the injected light emerges from the probed tissue due to absorption and strong scattering. The most common method for improving light collection is by optimizing the contact area between the detection system and the probed tissue by means of light guides with large detection surface.[15] Since the size of these light guides is not compatible with commercial spectrometers, which are typically equipped with an entrance slit to improve their spectral resolution, deep tissue spectrometers are usually custom-built.[10,14–16] Nevertheless, off-the-shelf spectrometers have attractive advantages compared to custom-made units, such as low cost, small footprint, and wide availability.[17] Some spectrometer manufacturers have attempted to tackle the issue of the compatibility with large detection light guides by removing the entrance slit and using a single fiber to guide light to the spectrometer.[18] This approach is, however, impeded by its inability to concomitantly provide good spectral resolution and large contact area

*Address all correspondence to: Mamadou Diop, E-mail: mdiop@lawsonimaging.ca

0091-3286/2014/$25.00 © 2014 SPIE

with the probed tissue. That is, either the spectrometer is equipped with a large-diameter fiber to optimize light collection, at the expense of spectral resolution, or a small-diameter fiber is used for good spectral resolution, at the expense of sensitivity.

In this paper, we propose an approach that provides high sensitivity, by improving light collection and reducing measurement noise, while maintaining good spectral resolution. Light collection was increased by removing the slit and using the output of the detection light guide as entrance to the spectrometer. To maintain good spectral resolution, the output of the fiber bundle was designed to mimic the typical form-factor of a spectrometer's entrance slit. The quality of the data was further improved by de-noising the measurements using a wavelet-based algorithm. The spectral resolution, wavelength accuracy, and noise characteristics of the modified instrument were quantified and compared to the specifications of a custom-built spectrometer that has been previously validated for deep tissue spectroscopy.[11] The ability of the modified spectrometer, augmented by the wavelet de-noising approach and differential spectroscopy data analysis, to quantify cerebral hemodynamics was illustrated in a piglet by measuring CBF and oxygen metabolism under different anesthetic regimens.

2 Materials and Methods

2.1 *Instrument Modifications*

The approach described here is of general purpose and can be applied to most off-the-shelf spectrometers, although the principle was demonstrated using the QE65000 unit from Ocean Optics, Dunedin, Florida. The spectrometer's slit was removed, to increase light throughput to the detector, so that the output of the detection fiber bundle became the entrance to the spectrometer. To maintain good spectral resolution, the output of the fiber bundle was designed to mimic the typical shape of an entrance slit; the proximal end of the fiber bundle was made of two columns of seven fibers (Fig. 1), forming a rectangular strip of $\sim 0.215\ \text{mm} \times 1\ \text{mm}$ (width $\times$ height). The tip of the fiber bundle with the rectangular output was positioned at the entrance of the spectrometer, with the two columns of fibers parallel to the vertical dimension of the CCD detector, and locked in place using an SMA905 connector. At the distal end of the bundle, the 125-μm core diameter silica fibers were closely packed (left of Fig. 1) to reduce the footprint of the probe. Note that the detection fiber bundle was custom built by Fiberoptics Technology, Inc. (Pomfret, Connecticut) according to the specific design requirements outlined above.

2.2 *Characterization of the Modified Spectrometer*

The spectral resolution and wavelength accuracy of the modified spectrometer were characterized and compared to the specifications of a custom-built unit that has been validated for deep tissue spectroscopy.[11,12] The latter was equipped with a front-illuminated CCD camera (S7010-1007, Hamamatsu Photonics, Bridgewater, New Jersey and Japan) cooled to −73°C by a four-stage Peltier cooling system (Wright Instruments Ltd, Enfield, United Kingdom).[13] At this temperature, the dark current was 7.7×10^{-3} electron/pixel/second and the mean readout noise was 6.9 counts. The CCD was operated as an array detector by binning the 124 pixels along the vertical direction.[13]

The detector of the off-the-shelf spectrometer was also a two-dimensional CCD array (Hamamatsu S7031-1006; 1044 columns by 64 rows of pixels, pixel size of 24 μm^2, detection range between 200–1100 nm, 90% quantum efficiency at 700-nm peak). Likewise, the pixels along the vertical dimension were also binned to operate the CCD as an array detector.[18] The major sources of noise (readout, shot, and dark noise) were characterized using an approach similar to the method described by Zonios.[19]

2.2.1 *Readout noise*

To measure the readout noise, the integration time was set to 8 ms—the fastest operating rate of the spectrometer—and the CCD detector was cooled to its lowest temperature (−20°C) to minimize dark noise. The photoelectron (shot) noise was also minimized by covering the entrance of the spectrometer so that no light reached the CCD detector. One hundred spectra were acquired successively in this configuration. The readout noise, defined as the standard deviation from the mean intensity of 100 measurements, was calculated for each pixel.

2.2.2 *Shot noise*

To evaluate the shot noise, the integration time was again set to 8 ms and the CCD temperature to −20°C. The output of a broadband light source (Ocean Optics HL-2000-HP) was adjusted by combinations of neutral density filters to obtain 13 different levels of light intensity. One hundred spectra were acquired at each intensity level. For every pixel, the mean and standard deviation (i.e., the noise) were calculated for each set of one hundred measurements. From these data, the detector gain and readout noise were calculated by fitting the measurements with the following equation:[19]

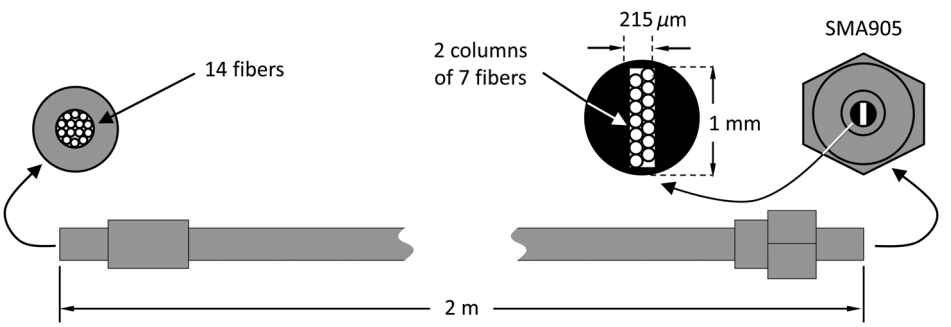

Fig. 1 Schematic of the detection fiber bundle; the 14 fibers (core diameter = 125 μm) were closely packed at one end (left) and arranged into two columns of seven fibers at the other end (right) to form a rectangular output acting as the spectrometer's entrance slit. The end of the fiber bundle with the rectangular strip was secured in front of the spectrometer with the SMA905 connector.

$$N = \sqrt{N_R^2 + S/G}, \tag{1}$$

where N is the measured noise which is composed of the readout noise (N_R), the mean signal intensity (S), and pixel gain (G).

2.2.3 *Dark noise*

Dark noise was evaluated by covering the entrance of the spectrometer, to minimize shot noise, and acquiring one hundred spectra at different integration times (8 ms to 20 s). In this configuration, the measured cumulative noise (readout noise and dark noise) can be modeled as[19]

$$N = \sqrt{N_R^2 + T \times n_d/G^2}, \tag{2}$$

where N is the measured noise, N_R is the readout noise, T is the integration time, G is the detector gain, and n_d is the dark electron accumulation rate. By measuring the standard deviation (at one pixel) for different integration times, the dark electron accumulation rate can be determined by fitting the measurement with Eq. (2). The dependence of dark noise on temperature was also evaluated by repeating the procedure with the CCD cooled from −10 to −20°C in step of 2°C.

2.2.4 *Stability test*

The stability of the modified spectrometer was also tested and compared to that of the custom-built unit. Spectra from a broadband the light source (Ocean Optics HL-2000-HP) were acquired continuously over an hour by each spectrometer using an integration time of 400 ms, the typical duration used in our *in vivo* measurements. The normalized standard deviation of the area under the spectra was calculated for each spectrometer to evaluate its stability.

3 Data Analysis

3.1 *Wavelet De-Noising*

The de-noising algorithm was adopted from our previous works.[20,21] First, the noise's variance was stabilized by applying the Anscombe transformation to the measured spectra.[22] This step efficiently transformed the Poisson noise in the data into white Gaussian noise. Second, the white noise was filtered out by wavelet de-noising using the MATLAB® function *wden* with Daubechies wavelets of order 10.[20] Finally, an inverse transformation (Anscombe inverse exact unbiased transformation) was applied to the de-noised data to obtain an estimate of the original noise-free spectra.[22]

3.2 *Quantification of Cerebral Chromophore Concentrations*

Near-infrared light propagation in turbid media can be described by the radiative transfer equation which, in the case of the present application, can be reduced to its diffusion approximation.[23] Since the extra-cerebral tissue layer in newborn piglets is very thin (1 to 2 mm), the head can be approximated as a semi-infinite homogeneous medium.[10] As such, the results presented in this paper were obtained by analyzing the piglet's head measurements using the following solution to the diffusion equation for a semi-infinite homogenous medium[10,24]

$$\psi = \frac{2S}{(4\pi)^2 D}\frac{\exp\left[-\rho\left(\frac{\mu_a}{D}\right)^{1/2}\right]}{\rho^3}\left[1+\rho\left(\frac{\mu_a}{D}\right)^{1/2}\right](z_0+z_b) \times\left\{z+3D\left[1-\frac{(z_0+z_b)^2+3z^2}{2\rho^2}\left(3+\frac{\rho^2\frac{\mu_a}{D}}{1+\rho\left(\frac{\mu_a}{D}\right)^{1/2}}\right)\right]\right\}, \tag{3}$$

where $D = 1/[3*(\mu_a+\mu_s')]$ is the diffusion coefficient, ρ is the radial distance between the emission and detection probes, S is the source strength in photon per second, μ_a and μ_s' are the absorption and reduced scattering coefficients, respectively, and z_0 and z_b are the boundary approximation parameters and are defined by the following expressions:

$$z_0 = (\mu_a+\mu_s')^{-1}, \tag{4}$$

$$z_b = \frac{1+R_{eff}}{1-R_{eff}}2D, \tag{5}$$

where R_{eff} represents the fraction of photons that is internally reflected at the boundary, and z_b was computed using the approach described by Haskell et al.[25]

Brain chromophore concentrations were quantified using a modified version of the method described in Ref. 10. First, the reflectance $R(\lambda)$ was calculated from the spectrum measured on the piglet's head, the dark spectrum of the spectrometer, and the reference signal obtained with the light source by

$$R(\lambda) = \log_{10}\left(\frac{\text{spectrum}_\lambda - \text{dark}_\lambda}{\text{reference}_\lambda - \text{dark}_\lambda}\right). \tag{6}$$

Next, the second spectral derivative of Eq. (3) was fit to the second spectral derivative of $R(\lambda)$ between 825 and 850 nm to extract the water concentration. The choice of this wavelength range was guided by previous findings showing that the second spectral derivative of the scattering coefficient and the other tissue chromophores do not change significantly in this spectral window.[26] The recovered water concentration was then used as a fixed parameter in the fitting of the first spectral derivative of $R(\lambda)$ with the first derivative of Eq. (3), to obtain the scattering coefficient and the remaining tissue chromophores. The objective function of the fitting was the norm of the difference between the measured and theoretical derivative spectra. However, instead of an exhaustive search, as in Ref. 10, a least-squares minimization routine based on *fminsearchbnd*[27] was developed to find the fitting parameters that minimized the objective function. This adaptation provided ~20-fold increase in the speed of the algorithm compared to the previous approach.[10] The fitting parameters included the concentration of oxy-hemoglobin (HbO_2), deoxy-hemoglobin (Hb), water (H_2O), and fat as well as the reduced scattering coefficient. The upper and lower boundaries of these parameters were set using a range that spans the published literature values for brain tissue and are shown in Table 1.[28] Note that both first and second spectral derivatives of the reflectance measurements and theoretical model were computed with a subroutine built in MATLAB® using the diff function. Furthermore, the goodness-of-fit was evaluated by computing the deviation of the measurements from the model, using the summed square of the residuals:

Table 1 Lower and upper limits of the fitting parameters, i.e., reduced scattering coefficient (μ_s') and concentrations of water (H_2O), deoxy-hemoglobin (Hb), and oxy-hemoglobin (HbO_2).

	H_2O (%)	Hb (μM)	HbO_2 (μM)	Fat (%)	μ_s' (mm^{-1})
Lower limit	70	5	10	0	0.4
Upper limit	90	40	80	50	1.5

$$\mathrm{SSE} = \sum_{n=1}^{N} (R_i - \hat{R}_i)^2, \tag{7}$$

where R_i is the measured quantity (first or second spectral derivative) and $\hat{R}_i$ is the corresponding theoretical prediction.

For the dynamic contrast-enhanced measurements (described in Sec. 4), the spectra acquired during the indocyanine green (ICG) injection were analyzed by fixing the scattering coefficient and endogenous chromophore concentrations to their pre-injection values (i.e., assuming that they did not change during the 2 min duration of the bolus-tracking experiment) so that the ICG concentration was the sole fitting parameter.

4 *In Vivo* Measurement

The animal experiments were conducted to illustrate the ability of the modified spectrometer, augmented by the wavelet de-noising and the spectral derivative approach, to measure CBF and oxygen metabolism in newborns. The study was approved by the Animal Use Subcommittee of the Canadian Council on Animal Care at Western University and was conducted according to its guidelines. A Duroc-cross piglet was delivered from a local supplier on the morning of the experiment. The animal was anaesthetized with 1.75% isoflurane (3% during surgery), tracheotomized, and mechanically ventilated on an oxygen/medical air mixture. A femoral artery was catheterized to monitor blood pressure and intermittently collect blood samples for gas and glucose analysis. An ear vein was catheterized to inject the light-absorbing intravascular tracer, ICG (Sigma-Aldrich, St. Louis, Missouri). The piglet was placed in the prone position and a probe holder was strapped to its head to hold the emission and detection probes at a separation of 3 cm. This separation has been shown to provide good sensitivity to the brain with probes positioned on the scalp.[29] The piglet was allowed to stabilize for 1 h after surgery before any measurements were acquired.

To investigate the effects of the noise reduction, one hundred spectra were acquired (while the animal was in stable condition) and de-noised. Thereafter, the two sets of data (raw and de-noised spectra) were analyzed with the method described in Sec. 3.2. The mean and standard deviation of the reduced scattering coefficient and cerebral chromophore concentrations, obtained from the two sets of spectra, were compared to reveal the effects of the de-noising.

Dynamic contrast-enhanced measurements were acquired while the piglet was subject to three different anesthetic regimens: isoflurane (2%), light isoflurane (0.75%) plus nitrous (2 L/min), and propofol infusion (3.0 mL/h). Hemodynamics measurements were acquired at each anesthetic level and required an intravenous bolus injection of ICG (0.05 mg dissolved in 0.5 mL sterile water). Tissue and arterial ICG concentration curves were concomitantly measured for 2 min by the modified spectrometer and a dye densitometer (DDG 2001, Nihon Kohden, Japan), respectively. CBF was calculated from these curves and combined with the tissue and arterial oxygen saturations to extract the cerebral metabolic rate of oxygen ($CMRO_2$), as previously described.[30]

5 Results

Figure 2 displays two spectra from the same neon light source measured by the modified spectrometer (QE65000) and the custom-built unit equipped with the S7010-1007 Hamamatsu CCD detector. This graph shows that subtle spectral features in the neon spectrum were better resolved by the modified spectrometer than the custom-built unit. For example, the neon spectrum measured by the modified spectrometer clearly showed one small peak at 718 nm and a higher one at 724 nm while these two peaks were not resolvable in the spectrum acquired by the custom-built unit. As well, the full-width at-half maximum of the highest peak (at 703 nm) and those of two other representative peaks (one on either side of the 703-nm peak) of the neon light source are displayed in Table 2. These results show that although the modified spectrometer has a relatively lower sensitivity than the custom-built unit in the 725- to 900-nm wavelength range, the spectral lines measured by the former were consistently narrower than those acquired with the latter. Since the spectral dispersion of both spectrometers was ~0.37 nm/pixel and they also have similar pixel size (~24 μm), the better resolution of the modified spectrometer is likely due to the slightly smaller width of the detection

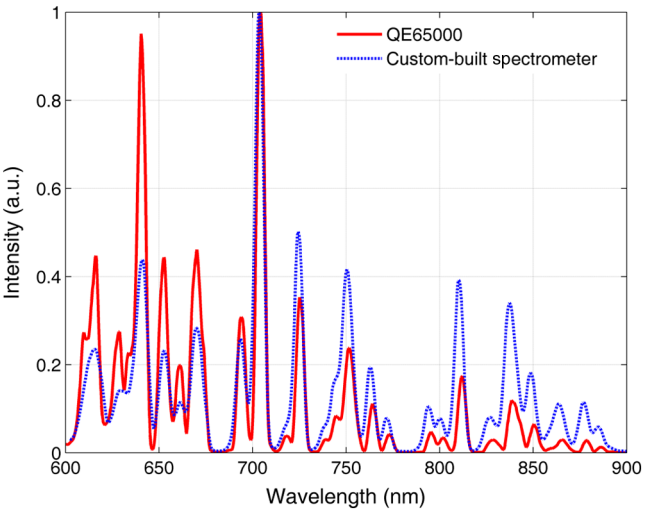

Fig. 2 Comparison of spectra from the same neon light source measured by the modified spectrometer and the custom-built unit.

Table 2 Full-width at half-maximum (FWHM) of the highest peak (at 703 nm) and those of two other representative peaks (one on either side of the 703-nm peak) of the neon light source measured by each spectrometer.

Peak position (nm)	640	703	811
Custom built spectrometer (FWHM in nm)	7.8	5.5	5.4
Modified spectrometer (FWHM in nm)	5.7	4.7	4.8

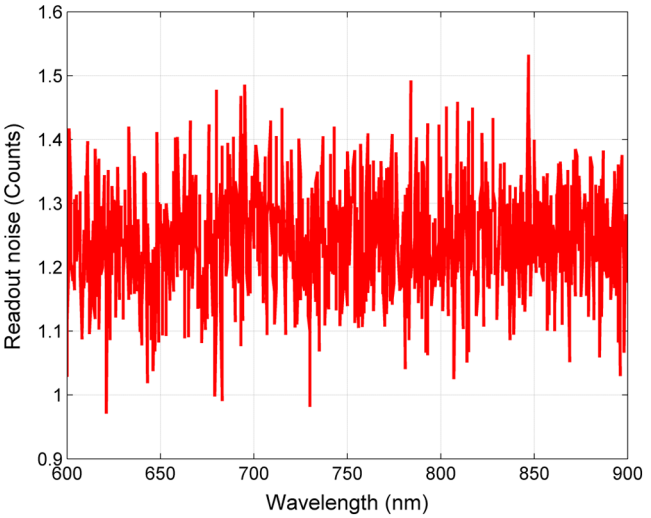

Fig. 3 Readout noise acquired at the shortest integration time (8 ms) with the CCD cooled to −20°C to minimize dark noise. The entrance to the spectrometer was also blocked to eliminate shot noise.

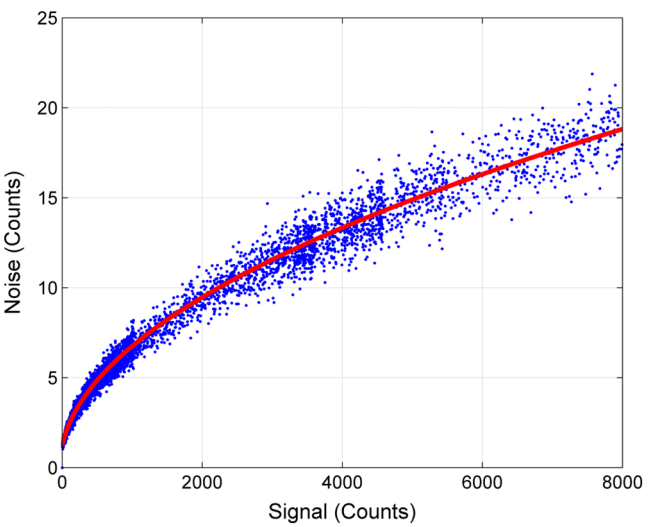

Fig. 4 Experimental noise (blue dots) plotted as a function of the mean signal intensity. The solid curve is the best fit of Eq. (1).

fiber bundle (∼215 μm) compared to that of the slit (∼250 μm) of the custom-built unit. Furthermore, the wavelength accuracy of the modified instrument was determined by comparing the positions of the spectral lines of a low-pressure mercury–argon calibration light source measured by the spectrometer to the values provided by the manufacturer. The results revealed that the modified spectrometer could measure the positions of the spectral lines with an accuracy of ∼1 nm over the entire wavelength range.

Figure 3 displays the readout noise measured with the CCD cooled to −20°C; the average value was ∼1.2 counts, in good agreement with the 1.5 counts provided by the manufacturer. Figure 4 shows the dependence of the shot noise on signal intensity; the solid curve is the theoretical prediction of Eq. (1) and the dots are the measured noise. The model fit yielded a detector gain (G) of 23 and a readout noise (N_R) of 1.2 counts, which is in excellent agreement with the value obtained from the data presented in Fig. 3.

Figure 5 depicts the expected dependency of dark noise on integration time and detector temperature. The dark electron accumulation rate (n_d) obtained by fitting the noise measurements with Eq. (2) was 251 and 84 counts^2/pixel/s at −10 and −18°C, respectively. Table 3 displays the readout noise and n_d at CCD temperatures from −10 to −20°C. As expected, the readout noise remained constant while there was a positive correlation between n_d and temperature. Figure 5(a) shows that at −10°C the measured noise was dominated by readout noise up to integration time of 0.6 s, while the dark noise quickly dominated for longer integration times. Cooling the CCD to −18°C extended the integration time up to 3 s without substantial increase in dark noise [Fig. 5(b)].

Figure 6(a) illustrates the noise in the raw measurements [same data as in Fig. 5(a)] and after de-noising. This figure demonstrates that de-noising reduced the readout noise from 1.3 to <0.5 counts, as evident by comparing the noise values for integration times <0.6 s. In addition, the total noise remained <1 count for higher integration times, showing that de-noising also reduced the dark electron accumulation rate. Figure 6(b) displays a reflectance spectrum from raw and de-noised data measured on the piglet's head; de-noising reduced the variability in the data without altering the shape of the reflectance curve. These graphs collectively show that the de-noising can

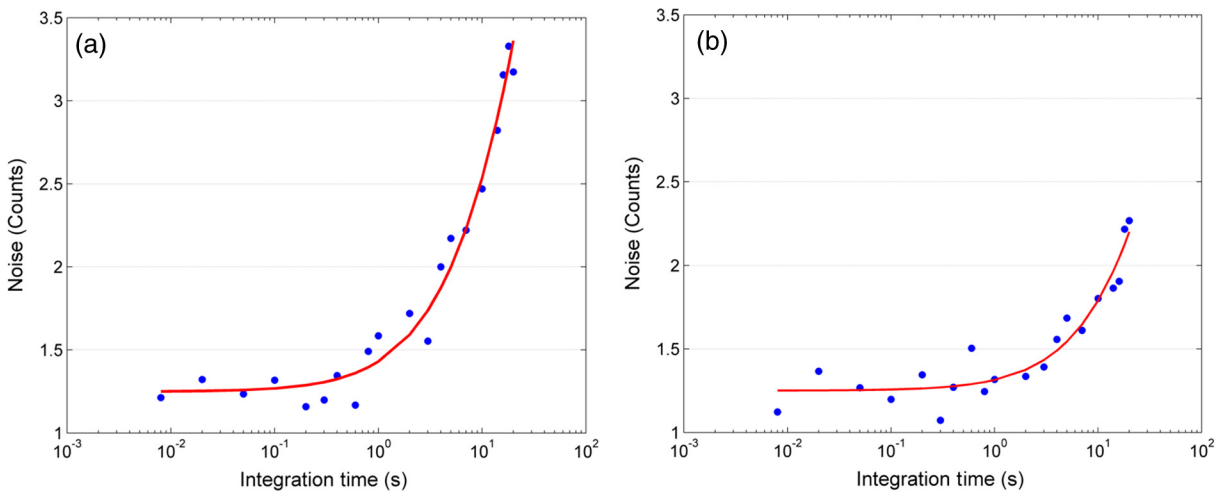

Fig. 5 The cumulative noise (i.e., readout and dark) in one pixel (blue dots) plotted as a function of integration time at (a) −10°C and (b) −18°C. The solid curves are the best fit to Eq. (2).

Table 3 Dark electron accumulation rate and readout noise measured at different temperatures of the CCD detector.

Temperature (°C)	N_R (counts)	n_d (counts^2/pixel/s)
−10	1.25	251
−12	1.24	181
−14	1.27	160
−16	1.26	121
−18	1.25	84
−20	1.24	66

efficiently reduce the three main sources of noise without altering the integrity of the data. Furthermore, the SSE of the residuals for the first spectral derivatives was 13×10^{-4} for the raw data and 8×10^{-4} for the de-noised spectrum, and for the second derivatives they were 7×10^{-5} and 3.5×10^{-5} for the raw and de-noised data, respectively. The consistent improved goodness-of-fit of the de-noised data for both the first and second spectral derivatives further confirms the ability of the de-noising algorithm to reduce measurement noise.

As a final note on the instrument characteristics, the stability test revealed that the normalized standard deviation from the mean intensity, over 1 h of measurements, was 1.4×10^4 and 7.9×10^3 for the custom-built spectrometer and the modified unit, respectively. This result indicates that the two instruments have similar stability.

The first and second spectral derivatives of a typical reflectance spectrum acquired on the piglet's head and the corresponding de-noised data are depicted in Fig. 7. Included in the graphs are the best fits to the spectral derivatives of the theoretical model. Table 4 shows the mean and standard deviation of the reduced scattering coefficient (at 800 nm) and cerebral concentrations of H_2O, Hb, and HbO_2, obtained by fitting the two sets of one hundred reflectance spectra (raw and de-noised). The mean values of the fitting parameters obtained from both sets of spectra were the same, but less variability was evident after de-noising. Note that we do not report fat concentration values since they were close to zero for both data sets, likely due to a lack of distinctive spectral features of this chromophore in the wavelength range covered by the spectrometer (see Sec. 6).

Figure 8 shows the ICG concentration curves measured under the three anesthetics. Since the amount of ICG injected was approximately the same for all measurements, these curves suggest that CBF was higher under isoflurane and lower under propofol. These qualitative observations are in agreement with the absolute CBF recovered from the ICG curves and displayed in Table 5. Furthermore, the $CMRO_2$ was higher under nitrous, the lightest anesthetic, and a lower $CMRO_2$ value was measured under propofol, which was the strongest anesthetic.

6 Discussion

In contrast to commercially available CW-NIRS units that are typically equipped with few wavelengths to monitor relative oxygenation, broadband CW-NIRS instruments have the ability to quantify the concentrations of tissue chromophores. As such, broadband CW-NIRS is an attractive alternative to other quantitative approaches, such as time-resolved and frequency-domain techniques because it is technically simpler and less expensive. The interest in quantitative techniques is increasing since they provide the ability to measure key parameters of cerebral physiology—CBF and cerebral oxidative metabolism—that are potentially more sensitive markers of brain health than relative oxygenation.[31–33] Broadband CW-NIRS has been successfully used to quantify cerebral oxygenation and hemodynamics in both experimental and clinical studies.[10,11,14,31,33–35] However, to date, all broadband CW-NIRS applications have involved custom-built spectrometers. Given that off-the-shelf spectrometers with good noise characteristics are becoming increasingly affordable, the focus of this work was to explore the feasibility of using such a spectrometer to quantify CBF and oxygen metabolism.

A general approach for improving the sensitivity of these spectrometers, while maintaining good spectral resolution and

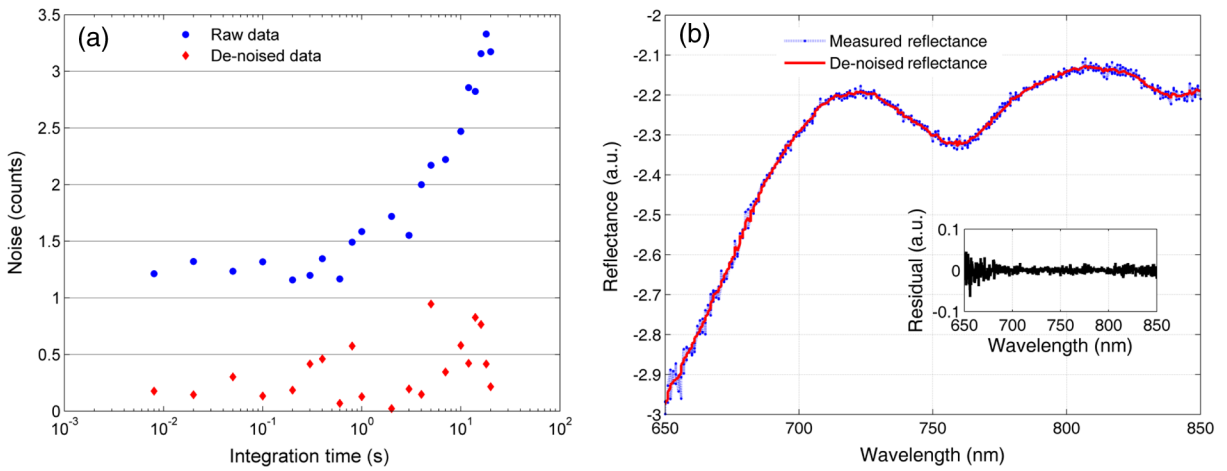

Fig. 6 (a) Effects of de-noising at different integration times with the CCD cooled to −10°C. The dots and diamonds are the noise in the raw data and after de-noising, respectively. (b) Reflectance spectrum obtained from the piglet's head before and after de-noising. The inset is the residual between the two reflectance spectra.

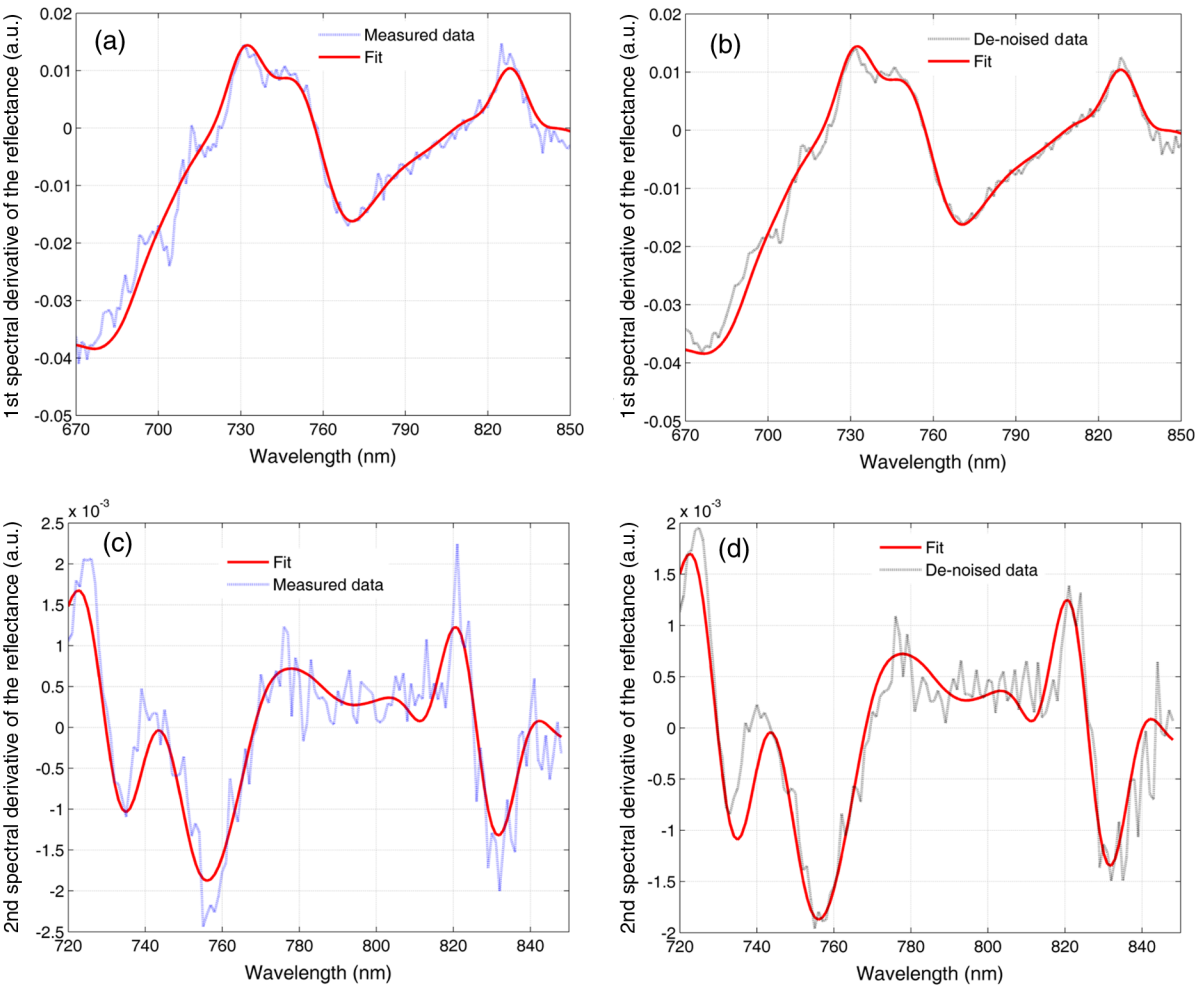

Fig. 7 First (a) and second (c) spectral derivatives of a typical reflectance spectrum measured on the piglet's head and the best fit to the model first and second spectral derivatives of the diffusion approximation. (b and d) Same data after de-noising with their corresponding fit to the model.

reducing the instrumental noise was introduced. The principle was illustrated with a compact low-cost spectrometer in which the entrance slit was removed to increase the light throughput to the detector. Removing the slit could potentially degrade spectral resolution and wavelength accuracy. To avoid these pitfalls while maintaining efficient light collection, which is critical in broadband NIRS, the modified spectrometer was

Table 4 Mean and standard deviation (SD) of μ_s' (at 800 nm), and concentrations of H_2O, Hb, and HbO_2 obtained by fitting each reflectance spectrum of the two data sets (raw and de-noised).

	Raw reflectance		De-noised reflectance	
	Mean	SD	Mean	SD
H_2O (%)	85	5	85	2
Hb (μM)	13	0.5	13	0.2
HbO_2 (μM)	26	5.3	25	2.1
μ_s' (mm^{-1})	0.79	0.09	0.79	0.05

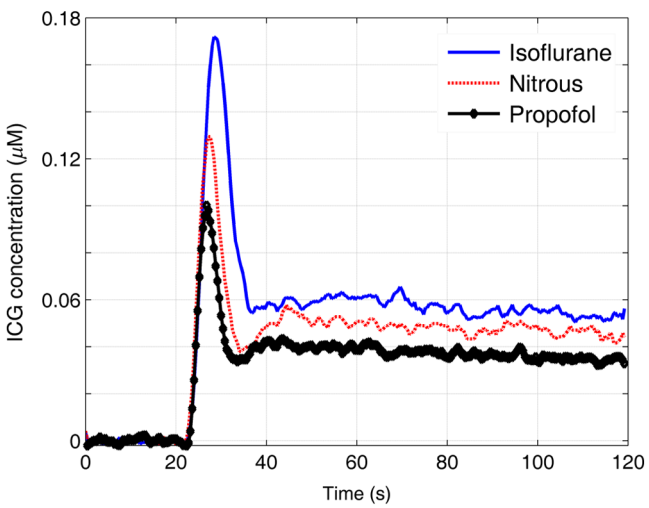

Fig. 8 Brain indocyanine green concentration curves measured under different anesthetic regimens.

Table 5 Cerebral blood flow (CBF), cerebral metabolic rate of oxygen ($CMRO_2$), oxy- and deoxy-hemoglobin concentrations, and tissue oxygen saturation (ScO_2) under different anesthetics.

	CBF (mL/min/100 g)	$CMRO_2$ (mL O_2/min/100 g)	Hb (μM)	HbO_2 (μM)	ScO_2 (%)
Isoflurane	29	1.5	14	25	65
Nitrous	25	1.8	15	16	51
Propofol	21	1.1	11	20	64

equipped with a detection light guide made of flexible optical fibers arranged in a configuration that mimics the typical form-factor of an entrance slit. This simple approach enabled to transform a low-cost spectrometer designed for dilute solutions into a suitable instrument for deep tissue spectroscopy as shown in this paper.

The modified spectrometer was characterized and the results showed that its spectral characteristics were comparable to those of a high quality custom-built unit, specifically designed for deep tissue spectroscopy (Fig. 2). Spectral accuracy was accessed by comparing the positions of the spectral lines of a calibration lamp measured by the modified spectrometer to the known values provided by the manufacturer of the light source. The wavelength accuracy of the instrument was found to be ~1 nm which is adequate for tissue spectroscopy, given the wide spectral features of HbO_2, Hb, H_2O, fat, and ICG in the near-infrared range.[36] As well, the similarity of the positions of the spectral lines of the neon light source measured by the two spectrometers (Fig. 2) is another illustration of the wavelength accuracy of the new instrument.

Since the modified spectrometer was equipped with a CCD array, the major contributors to detector noise were readout noise, photoelectron noise, and dark noise.[19,37,38] These noise components were quantified and the results showed that photoelectron noise was the main contributor. Note that in the photoelectron noise characterization, it was not possible to distinguish noise due to instability in the output power of the light source from pure shot noise. As such, the values of photoelectron noise reported here are, in fact, the combined contributions of both shot noise and light source instability. To further improve the noise characteristics of the system, all spectra were subsequently de-noised by a wavelet algorithm that was previously developed for time-resolved NIRS.[20] In this study, it was evident that de-noising spectral data improved the precision of the chromophore estimate (Table 4) with negligible effects on the shape of the reflectance spectrum (Fig. 6). Another important feature of the de-noising is its ability to significantly reduce dark noise even for integration times up to 20 s [Fig. 6(a)], which is appealing in low-light conditions such as at large source-detector separations in reflectance measurements or in the case of trans-cranial illumination. The de-nosing approach could also be adopted in other fields of optics dealing with weak spectrum measurements.[37]

One approach for quantifying cerebral chromophore concentrations from broadband CW-NIRS spectra is by second differential analysis.[39] Taking the second derivative of a spectrum removes the effects of scatter since it varies approximately linearly with wavelength. The differential pathlength and concentrations of chromophores can then be determined by assuming a known water concentration in brain, which is typically 80% to 90% depending on age and species.[35] However, a limitation with this approach is the inability to quantify the HbO_2 concentration due to the lack of any distinctive features in its second derivative spectrum.[8,39] A similar method that can quantify tissue HbO_2 concentration was proposed by Myers et al.[40] Their approach was based on an algebraic simplification of the second spectral derivative of tissue reflectance acquired at four wavelengths and required an empirical calibration with known tissue oxygen saturation. An alternative method that does not require any internal or empirical calibration is to model the wavelength-dependency of scatter with a power law and fit the broadband data with an analytical solution to the diffusion approximation.[10,41,42] In this paper, the fitting of the second spectral derivative was used to obtain the water concentration. The recovered H_2O concentration was subsequently used to constrain the fitting of the first derivative to obtain estimates of the other chromophores.

When applied to *in vivo* spectra, the second differential approach resulted in an estimated brain H_2O concentration of 85%, in agreement with the expected value.[39] As well, the reduced scattering coefficient and concentrations of Hb and HbO_2 recovered from the first derivative analysis were also in agreement with previously reported values.[43] Furthermore, the hemodynamics results were consistent with the relative strengths of the different anesthetics; the lowest $CMRO_2$ was measured under propofol, the strongest anesthetic. Although their physiological interpretation is beyond the scope of this paper, the CBF and $CMRO_2$ results illustrate the ability of this approach to quantify cerebral hemodynamics.

A limitation of this study is the lack of a direct comparison of the specs of the spectrometer before and after the modifications. Such information would certainly provide a quantitative assessment of the signal-to-noise ratio improvement provided by the modifications and confirm our qualitative observations. However, when compared to a similar (nonmodified QE65000) spectrometer, the detection efficiency of the modified spectrometer was approximately 45% higher. Another potential limitation is that in the data analysis, the piglet's head was treated as a semi-infinite homogenous medium. Although this is a rough approximation, such approach is widely used in the biomedical optics community to analyze NIRS measurements of neonates and piglets, and has been shown to produce blood flow estimates that strongly correlate with measurements obtained by state-of-the-art medical imaging modalities.[11,13]

A disadvantage with the low-cost spectrometer used in this paper was that it does not cover the 900 to 1000 nm spectral range. Since the absorption peak of fat is within this wavelength range, this spectrometer was unable to provide reliable estimates of tissue fat content. Nor can it be used to monitor tissue bound-water content or temperature by using the large water peak in this spectral window.[44–46] This limitation can, however, be mitigated by choosing an off-the-shelf unit that covers the 900 to 1000 nm spectral range or by slightly rotating the grating of the present spectrometer to encompass this wavelength range.

7 Conclusion

This study demonstrated that an off-the-shelf spectrometer can be easily modified to make it suitable for quantifying deep tissue chromophore concentrations. The noise and spectral

characteristics of the modified instrument were characterized and were found comparable to those of a custom-built spectrometer optimized for deep tissue spectroscopy. Combining the data analysis algorithms with the modified spectrometer provided a low-cost technique for measuring cerebral oxygenation and hemodynamics. Given the small footprint of these spectrometers, they could easily be adapted to intensive care units and also used as field-unit neuromonitors.

Acknowledgments

The authors would like to thank Jennifer Hadway and Laura Morrison for their assistance with the animal experiments and Anna Diop for her help in the instrument characterization. This research was supported by the Canadian Institutes of Health Research.

References

1. A. Sola et al., "Potential for protection and repair following injury to the developing brain: a role for erythropoietin?," *Pediatr. Res.* **57**(5), 110R–117R (2005).
2. G. Greisen, T. Leung, and M. Wolf, "Has the time come to use near-infrared spectroscopy as a routine clinical tool in preterm infants undergoing intensive care?," *Philos. Trans. R. Soc., A* **369**(1955), 4440–4451 (2011).
3. F. Gora et al., "Noninvasive measurement of cerebral blood flow in adults using near-infrared spectroscopy and indocyanine green: a pilot study," *J. Neurosurg. Anesthesiol.* **14**(3), 218–222 (2002).
4. H. Owen-Reece et al., "Use of near infrared spectroscopy to estimate cerebral blood flow in conscious and anaesthetized adult subjects," *Br. J. Anaesth.* **76**(1), 43–48 (1996).
5. J. T. Elliott et al., "Quantitative measurement of cerebral blood flow in a juvenile porcine model by depth-resolved near-infrared spectroscopy," *J. Biomed. Opt.* **15**(3), 037014 (2010).
6. F. Bevilacqua et al., "Broadband absorption spectroscopy in turbid media by combined frequency-domain and steady-state methods," *Appl. Opt.* **39**(34), 6498–6507 (2000).
7. M. Diop et al., "Comparison of time-resolved and continuous-wave near-infrared techniques for measuring cerebral blood flow in piglets," *J. Biomed. Opt.* **15**(5), 057004 (2010).
8. S. J. Matcher and C. E. Cooper, "Absolute quantification of deoxyhaemoglobin concentration in tissue near infrared spectroscopy," *Phys. Med. Biol.* **39**(8), 1295–1312 (1994).
9. S. J. Matcher, M. Cope, and D. T. Delpy, "Use of the water absorption spectrum to quantify tissue chromophore concentration changes in near-infrared spectroscopy," *Phys. Med. Biol.* **38**, 177–196 (1993).
10. H. Z. Yeganeh et al., "Broadband continuous-wave technique to measure baseline values and changes in the tissue chromophore concentrations," *Biomed. Opt. Express* **3**(11), 2761–2770 (2012).
11. D. W. Brown et al., "Quantitative near infrared spectroscopy measurement of cerebral hemodynamics in newborn piglets," *Pediatr. Res.* **51**(5), 564–570 (2002).
12. K. M. Tichauer et al., "Measurement of cerebral oxidative metabolism with near-infrared spectroscopy: a validation study," *J. Cereb. Blood Flow. Metab.* **26**(5), 722–730 (2005).
13. M. Diop et al., "A broadband continuous-wave multichannel near-infrared system for measuring regional cerebral blood flow and oxygen consumption in newborn piglets," *Rev. Sci. Instrum.* **80**(5), 054302 (2009).
14. R. Arora et al., "Preservation of the metabolic rate of oxygen in preterm infants during indomethacin therapy for closure of the ductus arteriosus," *Pediatr. Res.* **73**(6), 713–718 (2013).
15. R. Yang et al., "Monitoring angiogenesis using a human compatible calibration for broadband near-infrared spectroscopy," *J. Biomed. Opt.* **18**(1), 016011 (2013).
16. H. Xu et al., "Magnetic-resonance-imaging-coupled broadband near-infrared tomography system for small animal brain studies," *Appl. Opt.* **44**(11), 2177–2188 (2005).
17. E. Wright, K. St. Lawrence, and M. Diop, "Conversion of a low cost off-the-shelf spectrometer into a suitable instrument for deep tissue spectroscopy," *Proc. SPIE* **8573**, 85730V (2013).
18. Ocean Optics, "QE65000 Scientific-grade Spectrometer," http://www.oceanoptics.com/products/qe65000.asp (2010).
19. G. Zonios, "Noise and stray light characterization of a compact CCD spectrophotometer used in biomedical applications," *Appl. Opt.* **49**(2), 163–169 (2010).
20. M. Diop and K. St Lawrence, "Deconvolution method for recovering the photon time-of-flight distribution from time-resolved measurements," *Opt. Lett.* **37**(12), 2358–2360 (2012).
21. M. Diop and K. St Lawrence, "Improving the depth sensitivity of time-resolved measurements by extracting the distribution of times-of-flight," *Biomed. Opt. Express* **4**(3), 447–459 (2013).
22. M. Mäkitalo and A. Foi, "Optimal inversion of the Anscombe transformation in low-count Poisson image denoising," *IEEE Trans. Image Process.* **20**(1), 99–109 (2011).
23. F. Martelli et al., *Light Propagation through Biological Tissue and Other Diffusive Media: Theory, Solutions, and Software* SPIE Press, Bellingham, WA (2010).
24. S. Fantini, M. Franceschini, and E. Gratton, "Semi-infinite-geometry boundary problem for light migration in highly scattering media: a frequency-domain study in the diffusion approximation," *J. Opt. Soc. Am. B* **11**(10), 2128–2138 (1994).
25. R. C. Haskell et al., "Boundary conditions for the diffusion equation in radiative transfer," *J. Opt. Soc. Am. A* **11**(10), 2727–2741 (1994).
26. H. Zabihi-Yeganeh, "Non-invasive measurement of tissue chromophore concentrations and cerebral blood flow using broad-band continuous wave near infrared spectroscopy," Masters Thesis, Paper 1693 (2012).
27. J. D'Errico, http://www.mathworks.com/matlabcentral/fileexchange/8277-fminsearchbnd-fminsearchcon (6 February 2012).
28. S. L. Jacques, "Optical properties of biological tissues: a review," *Phys. Med. Biol.* **58**, R37–R61 (2013).
29. E. Okada and D. T. Delpy, "Near-infrared light propagation in an adult head model. II. Effect of superficial tissue thickness on the sensitivity of the near-infrared spectroscopy signal," *Appl. Opt.* **42**(16), 2915–2922 (2003).
30. K. Verdecchia et al., "Quantifying the cerebral metabolic rate of oxygen by combining diffuse correlation spectroscopy and time-resolved near-infrared spectroscopy," *J. Biomed. Opt.* **18**(2), 027007 (2013).
31. K. M. Tichauer et al., "Assessing the severity of perinatal hypoxia-ischemia in piglets using near-infrared spectroscopy to measure the cerebral metabolic rate of oxygen," *Pediatr. Res.* **65**(3), 301–306 (2009).
32. D. A. Boas and M. A. Franceschini, "Haemoglobin oxygen saturation as a biomarker: the problem and a solution," *Philos. Trans. R. Soc., A* **369**(1955), 4407–4424 (2011).
33. K. M. Tichauer et al., "Near-infrared spectroscopy measurements of cerebral blood flow and oxygen consumption following hypoxia-ischemia in newborn piglets," *J. Appl. Physiol.* **100**(3), 850–857 (2006).
34. T. S. Leung et al., "Theoretical investigation of measuring cerebral blood flow in the adult human head using bolus indocyanine green injection and near-infrared spectroscopy," *Appl. Opt.* **46**(10), 1604–1614 (2007).
35. C. E. Cooper et al., "The noninvasive measurement of absolute cerebral deoxyhemoglobin concentration and mean optical path length in the neonatal brain by second derivative near infrared spectroscopy," *Pediatr. Res.* **39**, 32–38 (1996).
36. S. Prahl and S. L. Jacques, "Optical properties spectra," http://omlc.ogi.edu/spectra/ (2001).
37. Z. Cai et al., "Quantification and elimination of the CCD dark current in weak spectrum measurement by modulation and correlation method," *Proc. SPIE* **7850**, 785005 (2010).
38. J. J. Davenport et al., "Noise analysis of a CCD based ultra-violet spectrometry system," *Proc. SPIE* **8439**, 84391P (2012).
39. R. Springett, Y. Sakata, and D. T. Delpy, "Precise measurement of cerebral blood flow in newborn piglets from the bolus passage of indocyanine green," *Phys. Med. Biol.* **46**(8), 2209–2225 (2001).
40. D. E. Myers et al., "Noninvasive method for measuring local hemoglobin oxygen saturation in tissue using wide gap second derivative near-infrared spectroscopy," *J. Biomed. Opt.* **10**(3), 034017 (2005).

41. R. Nachabé et al., "Estimation of lipid and water concentrations in scattering media with diffuse optical spectroscopy from 900 to 1,600 nm," *J. Biomed. Opt.* **15**(3), 037015 (2010).
42. O. Pucci, V. Toronov, and K. St Lawrence, "Measurement of the optical properties of a two-layer model of the human head using broadband near-infrared spectroscopy," *Appl. Opt.* **49**(32), 6324–6332 (2010).
43. S. Ijichi et al., "Quantification of cerebral hemoglobin as a function of oxygenation using near-infrared time-resolved spectroscopy in a piglet model of hypoxia," *J. Biomed. Opt.* **10**(2), 024026 (2005).
44. S. H. Chung et al., "In vivo water state measurements in breast cancer using broadband diffuse optical spectroscopy," *Phys. Med. Biol.* **53**(23), 6713–6727 (2008).
45. S. H. Chung et al., "Non-invasive tissue temperature measurements based on quantitative diffuse optical spectroscopy (DOS) of water," *Phys. Med. Biol.* **55**(13), 3753–3765 (2010).
46. S. H. Chung et al., "Non-invasive measurement of deep tissue temperature changes caused by apoptosis during breast cancer neoadjuvant chemotherapy: a case study," *J. Innovative Opt. Health Sci.* **4**(4), 361–372 (2011).

Biographies of the authors are not available.